Luminescence modulation in liquid crystalline phases containing a dispiro[fluorene-9,11'-indeno[1,2-b]fluorene-12',9"-fluorene] core

Sebastien Thiery, Benoît Heinrich, Bertrand Donnio, Cyril Poriel, Franck Camerel

Luminescence modulation in liquid crystalline phases containing a dispiro[fluorene-9,11'-indeno[1,2-*b*]fluorene-12',9''-fluorene] core

Sébastien Thiery,[a] Benoît Heinrich,[b] Bertrand Donnio,[b,c,*] Cyril Poriel[a,*] and Franck Camerel[a,*]

[a] Institut des Sciences Chimiques de Rennes, UMR 6226 (CNRS-Université de Rennes 1), Campus de Beaulieu, 35042 Rennes, France.

E-mail: cyril.poriel@univ-rennes1.fr; franck.camerel@univ-rennes1.fr

[b] Institut de Physique et Chimie des Matériaux de Strasbourg (IPCMS), UMR 7504 (CNRS-Université de Strasbourg), 23 rue du Loess, BP 43, 67034 Strasbourg Cedex 2, France.

[c] Complex Assemblies of Soft Matter Laboratory (COMPASS), UMI 3254 (CNRS-Rhodia/Solvay-University of Pennsylvania), CRTB, 350 George Patterson Boulevard, Bristol, PA 19007, USA.

Email : bdonnio@ipcms.unistra.fr

Abstract

A luminescent liquid crystalline compound containing a bulky dispiro[fluorene-9,11'-indeno[1,2-*b*]fluorene-12',9''-fluorene] has been designed and synthesized by di-substitution of a bromo derivative with N-(4-ethynylphenyl)-3,4,5-tris(hexadecyloxy)benzamide fragments. This di-substituted 3π-2spiro derivative forms stable and well-organized mesophases over large temperature ranges. Combination of DSC, POM and SAXS analyses has revealed the formation of a lamellar mesophase between 60 and 150 °C followed by another mesophase with a 2-dimensional lattice of rectangular symmetry that remains up to the isotropization point near 225 °C. In the original molecular packing model deduced from SAXS, the tert-butyl terminal groups fill the centre of hollow columns constituted by both the

dihydro(1,2-*b)*Indenofluorene and benzamide fragments and separated from each other by the surrounding aliphatic tails. The merging of the columns yielding the lamellar phase turned out to be governed by the dynamics of both, the micro-phase segregation process and the network of hydrogen bonds. In the various mesomorphic states and in solution, a strong luminescence was observed. The emission spectrum however depends on temperature and drastically changes between both mesophases and the isotropic liquid. In particular, a strong modulation of the emission wavelength occurs at the isotropic to 2D phase transition. This luminescence modulation results from an enhanced contribution of the vibronic peaks at lower energies in the emission profile. The compound was also found to be soluble in 5CB and was integrated in a guest-host LC cell, allowing modulating efficiently the photoluminescence polarization, in the presence or absence of an electrical field.

Introduction

Spiro compounds have been widely used in Organic Light Emitting Diodes (OLED) since their first incoporation in 1997 by the Salbeck group.[1] Of particular interest in this wide family of chromophores are the "3π/2spiro" compounds which are constituted of three π-systems linked by two spiro bridges. [2, 3, 4] This type of 3π-2spiro molecular structure can lead to fluorophores possessing very different properties depending on the geometry of the molecular scaffold or π-systems.[5] As an example, the association of a dihydroindeno[1,2-*b*] fluorenyl or a pentaphenylenyl core to two fluorenyl or xanthenyl units via two spiro bridges allowed obtaining efficient emitters for blue OLED applications.[2, 4, 6, 7] A further modification of the geometry of the molecular scaffold recently opened a new avenue to produce blue light in OLEDs through the use of intramolecular excimer emission.[8] Although, the incorporation of these molecules in a liquid-crystalline architecture could be a way to modulate their exceptional luminescence properties, no mesomorphic materials incorporating the

dispiro[fluorene-9,11'-indeno[1,2-*b*]fluorene-12',9"-fluorene] (DSF-IF) segments were reported up to date, to the best of our knowledge.

Yet, the mesomorphism would not only lead to the modulation of the photoluminescent properties, but also allow switching between several states in response to various external stimuli, which would be of great interest due to their potential application for memory devices, sensors and informational displays.[9] Indeed, electric-field controlled photoluminescence switching has been achieved in many systems by adding dyes into liquid crystalline hosts,[10] evidencing the potential interest of neat photoluminescent liquid crystalline materials.[11]

Thus, the present work investigates this concept and demonstrates that the DSF-IF scaffold can be efficiently functionalized to generate mesophases with strong luminescence properties. In order to reach this goal, a protomesogenic fragment, which has been already successfully used with pyrene derivatives to promote mesogens and molecular gelators,[12] was grafted on a DSF-IF derivative (Figure 1). Hydrogen bonding amides allow then the emergence of molecular self-assemblies stable over large temperature ranges.

In addition to the original temperature-dependent bulk luminescence properties, the potential application of such anisotropic materials in guest-host LC systems was also evaluated. For this purpose, the material was dissolved in the standard nematic liquid crystal matrix 5CB (4-cyano-4′-n-pentyl-1,1′-biphenyl) and we have demonstrated that marked photoluminescence polarization and modulation responses can obtained from the DSF-IF derivative in LC cells.

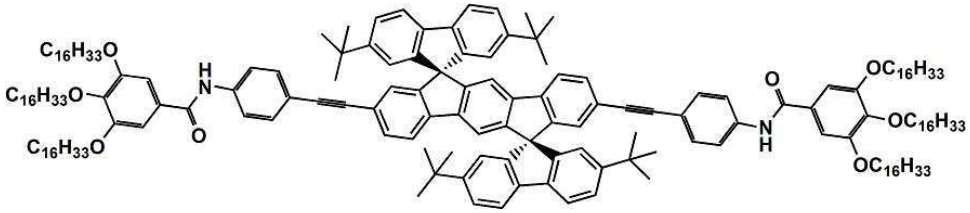

Figure 1. Chemical structure of the liquid crystalline compound **1** based on a

dispiro[fluorene-9,11'-indeno[1,2-*b*]fluorene-12',9"-fluorene] scaffold.

Results and discussion

Synthesis

The synthesis of **1** (Scheme 1) starts with the preparation of the key precursor, namely 2,2",7,7"-tetra-*tert*-butyldispiro[fluorene-9,6'-indeno[1,2-*b*]fluorene-12',9"-fluorene] (DSF-IF(t-Bu)$_4$), constituted of a dihydroindeno[1,2-*b*]fluorenyl core linked via spiro bridges to two 2,7-tert-butyl fluorenyl moieties. As previously reported, electrophilic bromination of DSF-IF(t-Bu)$_4$ leads to the dibromination of the dihydroindeno[1,2-*b*]fluorenyl core providing DSF-IF(*t*-Bu)$_4$Br$_2$ in high yield (90%).[13] The lipophilic alkyne moiety (EPBA) was synthesized in two steps from 3,4,5-tris(hexadecyloxy)benzoic acid chloride and 4-trimethylsilylethynylaniline.[12] Then, compound **1** was finally obtained in good yield (46%) via a palladium(0)-catalyzed cross-coupling reaction between DSF-IF(*t*-Bu)$_4$Br$_2$ and N-(4-ethynylphenyl)-3,4,5-tris(hexadecyloxy)benzamide in *n*-propylamine as base and solvent. The EPBA fragment, carrying an amide function, was selected preferentially to a half-disk moiety as the terminal group in order to introduce hydrogen bonding which is known to strongly stabilize supramolecular organisations over larger temperature range.[12]

The molecular structure and purity of **1** were confirmed using ^{1}H, ^{13}C NMR and mass spectroscopy. A set of aromatics peaks integrating for even numbers of protons confirmed the formation of the expected molecular structure and the symmetrical substitution pattern on the 2,8 positions of the dihydroindeno[1,2-*b*]fluorenyl scaffold.

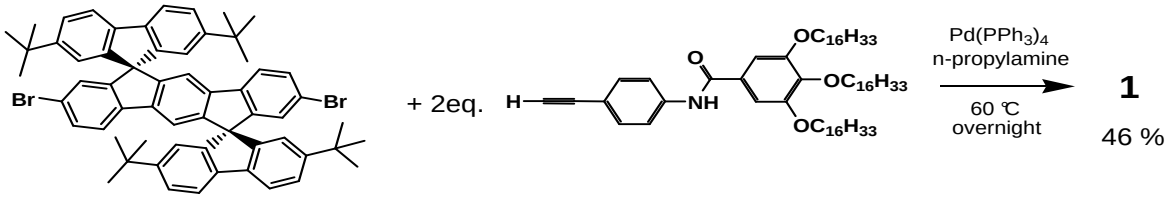

Scheme 1. Synthetic route for the preparation of **1.**

Spectroscopic Characterizations in Solution.

UV-Vis spectrum of **1** presents two main bands at 379 and 399 nm leading to a wide optical energy gap of ca 2.98 ev (Figure 2). The maximum appears hence to be strongly bathochromically shifted by ca 52 nm compared to that of its constituting building block DSF-IF(t-Bu)$_4$, leading to an impressive gap contraction (3.49 eV vs 2.98 eV).[14] This red shift is assigned to the extension of the π-conjugation induced by the presence of the N-(4-ethynylphenyl) fragment in *para* position of the phenyl-phenyl linkage of the dihydroindeno[1,2-*b*] fluorenyl core. Thus, the optical properties of **1** are almost fully governed by the ‘‘N-(4-ethynylphenyl)/dihydroindeno[1,2-*b*]fluorene/N-(4-ethynylphenyl’’ moiety, the electronic density of both Highest Occupied and Lowest Unoccupied Molecular Orbitals (HOMO and LUMO respectively) being distributed on this fragment (Figure S1). This extension of the π-conjugation appears to be relatively efficient through the rigid triple bond linkage. For example, compared to another structurally related extended DSF-IF derivative substituted on the dihydroindeno[1,2-*b*]-indenofluorenyl core by two 3,4,5-trimethoxyphenyl moieties (λ_{max} =362 nm, ΔE= 3.17 eV),[8] the present chromophore **1** appears to possess a smaller energy gap due to its extended π-conjugation (Figure S1). To the best of our knowledge, this is one of the most contracted energy gap observed in the literature for a DSF-IF derivative.[2]

Additionally, **1** presents an intense blue fluorescence with a well resolved spectrum presenting several maxima at 411, 435 and 467 nm (Figure 2). These maxima are strongly red shifted (59 nm) compared to those of its constituting building block DSF-IF(tBu)$_4$ (λ = 352 and 370 nm),[14] highlighting again the interest of the π-conjugation extension to obtain a blue emitter. The well-resolved emission spectrum of **1** compared to its absorption spectrum suggests a more rigid/planar structure of **1** in the excited state. Indeed, for species that comprise torsional

degrees of freedom in their π-conjugated backbones, varying degrees of deviation from the classical mirror image behaviour can be observed. Such differences between absorption and emission band-shapes may be associated to the flexible nature of the molecules (and in the present case especially the flexibility of the chains).[15] However, the Stokes shift defined as λ_{abs}-λ_{em} of **1** appeared to be small (12 nm), highlighting small rearrangements in the excited state. Thus, despite the presence of the flexible pendant N-(4-ethynylphenyl)-3,4,5-tris(hexadecyloxy)benzamide, which may lead to important rotational freedom, we note that the absorption spectrum and more importantly the fluorescence spectrum are well resolved, which is indicative of a very rigid molecular structure. Finally, the quantum yield of **1** has been measured at *ca* 0.32 compared to quinine sulphate (Figure S2 and Table S1). This value appears to be significantly decreased compared to that observed for DSF-IF(tBu)$_4$ (0.52 in CH_2Cl_2) and may be assigned to the introduction of the flexible N-(4-ethynylphenyl)-3,4,5-tris(hexadecyloxy)benzamide which may lead to non radiative de-activation process as often observed.[16] The perfect match between the excitation spectrum and the absorption spectrum points to an efficient radiative deactivation of the excited electronic state.

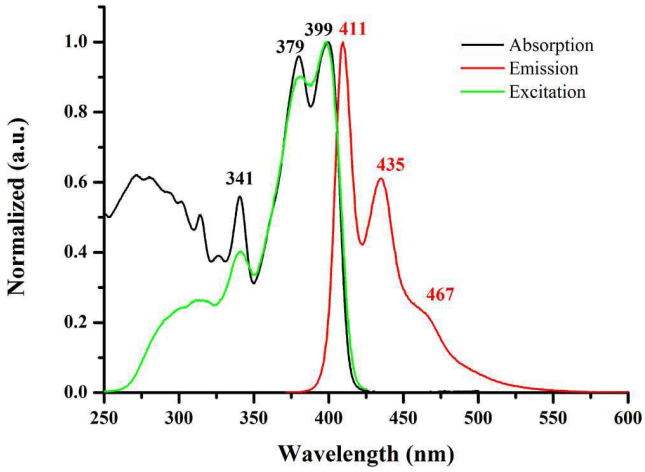

Figure 2. Absorption, emission (λ_{ex} = 358 nm) and excitation (λ_{em} = 435 nm) spectra of compound **1** in dichloromethane (c = 8.7 x 10^{-7} mol.L^{-1}).

Thermal behavior

Thermal and polymorphic behavior of **1** was investigated by differential scanning calorimetry (DSC) and polarized optical microscopy (POM). DSC analyses show that the compound exhibits three reversible main first order thermal transitions centred at 60, 150 and 225 °C (Figure S3). Above 225 °C, the compound is in its isotropic state. On cooling from the isotropic liquid, large birefringent domains readily develop over the whole film (Figure 3), whilst the soft texture is indicative of a mesomorphic state (referred thereafter to high-temperature, HT, phase, vide infra) (Figure S4, S5). Despite numerous efforts, no characteristic textures could have been developed; although, the texture is fluid and homogeneous, suggesting the formation of a LC phase. Successive transitions crossed on cooling down to room temperature were not associated to visible changes in the optical texture, from which no further information on the structure of the phases could be deduced (Figure S5). Nevertheless, the quite high fluidity of the sample between 60 and 150 °C indicates that the intermediate phase consists in a “low-temperature” (LT) mesophase, whilst the texture stiffens below the low-temperature transition and leaves the nature of the room-temperature state unclear.

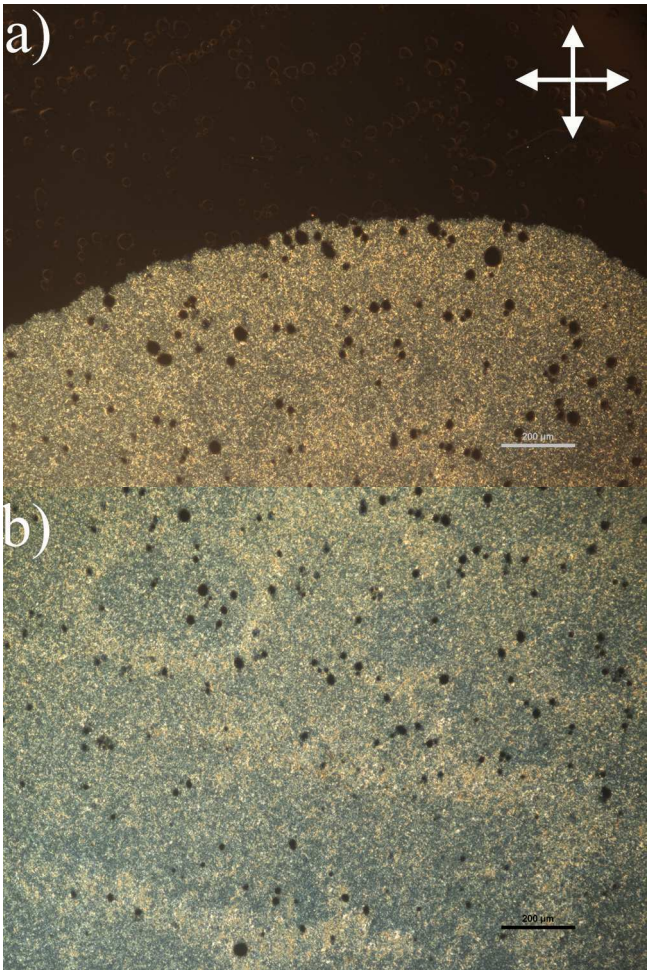

Figure 3. Compound **1** viewed by optical microscopy under crossed-polarisers upon cooling (symbolised by the cross in the corner of the picture) at a) 195 °C (co-existence of the isotropic liquid and HT phase) and b) HT phase at 180 °C (black spots correspond to air trapped bubbles).

Characterization by Small-angle X-ray scattering (SAXS)

The structures of the various phases were investigated, and identified by SAXS measurements.

The pristine (initial) state possesses a local "embryonic" lamellar organization evidenced by the presence of 6 broadened small-angle reflections in the ratio 1:3:4:5:6:10 (00*l*) and unresolved broad scattering signals in the wide-angle region (Figure S6, Table S2). After

heating the sample in the isotropic liquid, this poorly-organized state is restored on cooling down to room-temperature (diffractogram not shown).

Above the first transition, the broadened reflections of the room-temperature state are replaced by nine sharp reflections in the spacing ratio 1:2:3:4:5:6:7:8:10 (00*l*), according to a lamellar periodicity of 54.0 Å (see Figure 4a and Table S3). The wide-angle region only contains overlapping broad scattering signals, due to distances between segregated molecular fragments, particularly the characteristic scattering maximum at about 4.5 Å of molten aliphatic chains (h_{ch}) that confirms the assignment to a mesophase. The dominating (001) reflection trivially results from the alternation of sub-layers of mesogens and molten chains, but here the number of harmonics is unusually high, and therefore the interfaces between sub-layers unusually sharp. With this high degree of cohesion of the mesogens' sub-layers, it would not be surprising that a 3D structure persists in spite of the intercalation of the liquid aliphatic sub-layers. The unresolved shoulders in the mid- and wide-angle region might be the residue of such a vanishing structure, but the data collected do not permit to confirm such an assumption. The structure of the lamellar packing is characterized by the molecular area S, ratio of the molecular volume and layer spacing, $S = V_{mol}/d$. The estimation, that a density at 80°C lies approximately in the range 0.9-1.0 g. cm^{-3}, leads to area S comprised between 80 and 95 $Å^2$, i.e. slightly more than the cross-sections of three molten terminal chains (~68 $Å^2$): the diverging chains are therefore disordered and folded in order to compensate for the large molecular area imposed by the bulky rigid parts.

Finally, in the upper temperature range above 150°C, a complex diffraction pattern is produced, which remains unchanged up to the isotropization (ca 225 °C). Now, 21 sharp reflections (Figure 4b) could be precisely measured and satisfactorily indexed (Table S4) according to a centred rectangular lattice, and thus the mesophase is assigned as Col_{rec}-*c*2*mm*. Consequently, this transition corresponds to a lamellar-to-columnar phase transformation.

The high number of crossed (*hk*) reflections shows that the structure is perfectly defined along several directions of the lattice plane, and the modulation of their intensity suggests an additional segregation process likely between the lateral tert-butyl groups and the terminal chains (i.e. the lattice contains more than one peak of electronic density suggesting alternation of high- and low-electronic density fragments, vide supra). Four (*hk*) reflections are visible along two main axes of the columnar rectangular network, namely (20), S, (40), MW, (60), S, (80), M, and (11), VS, (22), S, (33), M, (44), W (Table S4) (VS, S, M, MW, W, VW stand for very strong, strong, medium, medium-weak, weak, very weak and correspond to the reflection intensities). The latter series, (*hh*), dominates largely over the former one, (*h*0), an indication of a strong anisotropy within the lattice plane. Moreover, the intensity of the (*hh*) reflections decreases regularly with h, in contrast to the (*h*0) series, for which the intensity goes through a minimum for the first harmonics. A second intensity minimum is found in the perpendicular direction to the (h0) series, (0 2k) (e.g. (02), S, (04), W, (06), absent, (08), M, Table S4), associated to an increase of the electronic density between the nodes of the network. Finally, in the other directions of the lattice plane, the first, high order reflection (31) is absent, and two higher order reflections, (13) and (51), are either absent or too weak, respectively, but the third one is intense ((42), S, (84), S), confirming the strong anisotropy in the plane, and the modulation of the electronic density. This detailed analysis shows that the variation of the intensity of the various reflections sets is compatible with a model of hollow columns (vide infra).

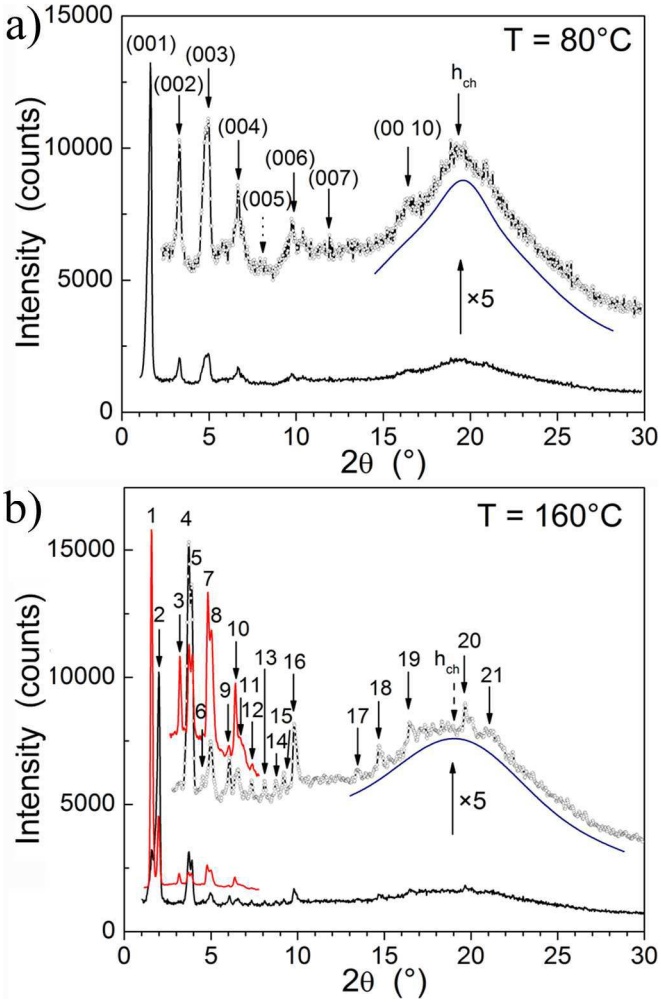

Figure 4. X-ray diffractograms of compound **1** recorded at 80°C (LT or lamellar phase) and at 160°C (HT or rectangular phase). In b) the superposed diffractogram was recorded on a synchrotron line (red), showing the good agreement between both techniques.

Supramolecular organization in the mesophases

A model for the mesophase structure consisting of the assembly of "hollow" columns is a priori not unexpected from the similar electronic density of tert-butyl groups and terminal chains on the one hand, and from the contrast with the high electronic densities of rigid fragments, on the other hand. The presence of aliphatic moieties at all mesogen ends could then leads to such a type of stratified structure. A more detailed inspection of the packing and supramolecular organization needs additional information about the molecular conformation

and geometry that could be extracted from a reference crystalline structure (structure from the Cambridge Structural Database, CSD number: XIVHEQ). The model compound bears the same tert-butyl-fluorene (TBF) and dihydro(1,2-*b)*Indenofluorene (InF) fragments as compound **1**, but without the terminal N-(ethynylphenyl) benzamide (EPBA) fragments and the terminal alkoxy chains. This molecular structure directly gives access to both TBF and InF dimensions and confirms the "double cross-like" molecular conformation.

The crystalline structure resulting from such a special geometry is very informative and consists in the superposition of the InF fragments associated in dimers, decorated by the TBF orientated along the self-assembled columns, that drives the segmentation of the columns by the tert-butyl groups, themselves segregated into layers. Similar processes of segregation as those occurring within the crystalline structure may explain the formation of the mesophase with hollow columns. In both cases (i.e. Col_{rec} mesophase and crystalline structure), the formation of the columns results from the piling of the InF segments, though in the mesophase, the columns are oriented parallel to the b-direction, in order to allow the layers containing the tert-butyl groups to be oriented along the a-axis, and to be evenly disrupted by the EPBA groups at the extremities of the InF fragments. Half of the tert-butyl-containing layers are thus segregated into ribbons, and surrounded by a continuous shell of rigid parts. The long aliphatic chains, accordingly to the segregation process found in polycatenar systems,[17] are folded around the columns, and form a continuum, which here is also fused with the other half of tert-butyls expelled out of the columns (Figure 5).

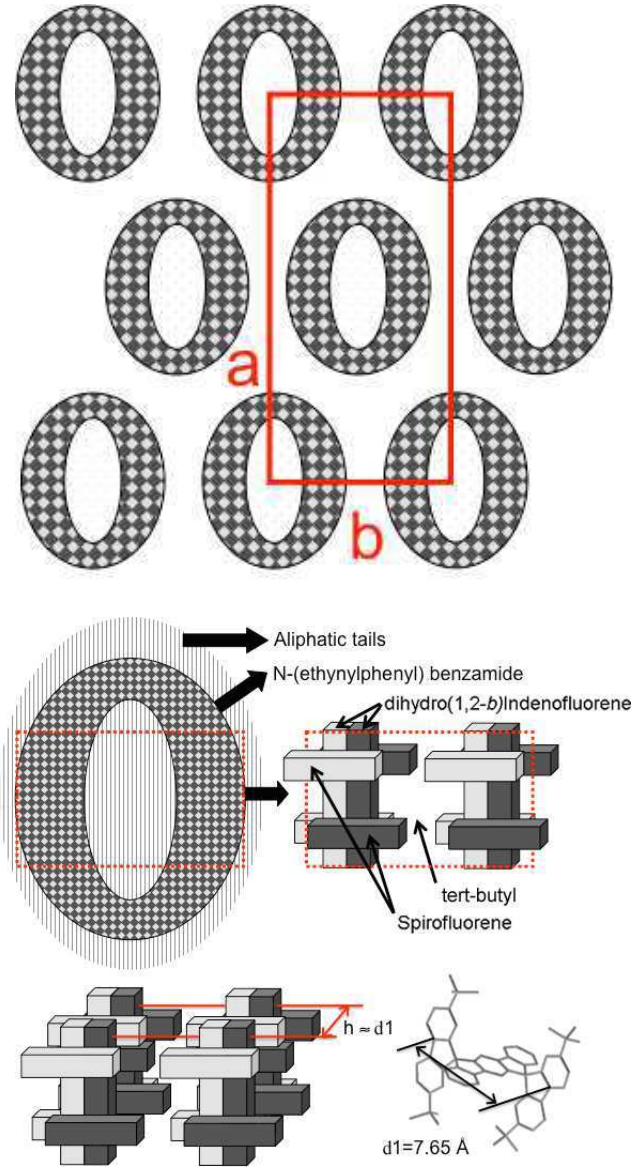

Figure 5. Model of the hollow columns and columnar rectangular phase formed by **1**.

Steric constraints associated to the molecular geometry and the multiple segregation process imply that the columnar cross-sections is defined by a precise integer number of molecules, in contrast to average statistical numbers in classical polycatenar systems. This specificity permits to understand the well-defined nature of the structure and the sharp interfaces between rigid parts and chains, at the origin of the large number of high order terms and crossed reflections in the diffractogram. This number is equal to Z/2 = 4 molecules per columnar repeat units. Estimating the molecular volume (V_{mol} = 4845 Å^3 at 160°C), one can now access

to the thickness of an elementary fictitious repeat unit according to $h = Z.V_{mol}/a.b = \sim 7.2$ Å, not to different to the distance between TBF segments (d1 ~ 7.65 Å) found in the crystalline structure of the model compound (even comparable, since the long aliphatic chains are not involved here). Organization along the columns can be assimilated to the alternation of monolayers of InF segments and of monolayers of intercalated TBF segments.

Superposition of the Col_{rec} and the lamellar phases diffraction patterns reveals that the reflections series (*h*0) (*h* = 2n) coincide with the reflections series (00*l*), except that the former are more intense, the intensity ratio are different and that all crossed reflections have disappeared. Nevertheless, it shows that the structure of the lamellar phase is not greatly different to that of the rectangular phase, except that the columns are not closed in the lamellar phase. The modulations in the lamellar planes due to the alternation of the fluorene segments and the tert-butyl groups likely pre-exist in the lamellar phase, but are not correlated over long distances, in agreement with the slight peak enlargement observed in the X-ray pattern.

The dynamic of the hydrogen bonding network was probed by variable-temperature FT-IR absorption spectra for compound **1** dispersed into KBr pellets. Measurements obtained upon heating and cooling (Figure 6 and Figure S7) show reproducible and reversible spectral changes of the bands associated to the amide functions at the phase transitions. A weakening of the out-of-plane NH bending band (amide V) localized at 720 cm^{-1} [18] is observed between the poorly organized room temperature phase and the lamellar phase and this vibration mode, associated to hydrogen bonded amide functions, completely disappear in the rectangular phase. The collapse of the hydrogen bonding network in the rectangular phase is further confirmed by the frequency and profile changes of the C=O stretching vibration (amide I) above 150 °C. In lamellar phase, the C=O stretching vibration appears as a single band at 1645 cm^{-1} and is characteristic of H-bonded amides.[19] Above 150 °C, the shift of this vibration

mode to higher frequencies is indicative of the disruption of the hydrogen bonds. A similar behaviour is found for the νN-H stretching vibrations vibration around 3300 cm^{-1}.[18, **Erreur ! Signet non défini.**] The major perturbations of the energy and intensity of the ν_{CO}, ν_{NH} and δ_{NH} stretching and deformation vibrations observed highlight that the hydrogen bonding network present in the lamellar phase is disrupted above 150 °C when entering into the rectangular phase.

The phase transitions appear to be strongly governed by the dynamic of the hydrogen bonding network. The presence of persisting hydrogen bonds in the lamellar phase forbids the folding of the chains at the EPBA extremity, and the transition to the Col_{rec} phase is connected to the collapse of the H-bonding network. Similarly, at low temperature, this H-bonded edifice would also perturb the lamellar supramolecular arrangement.

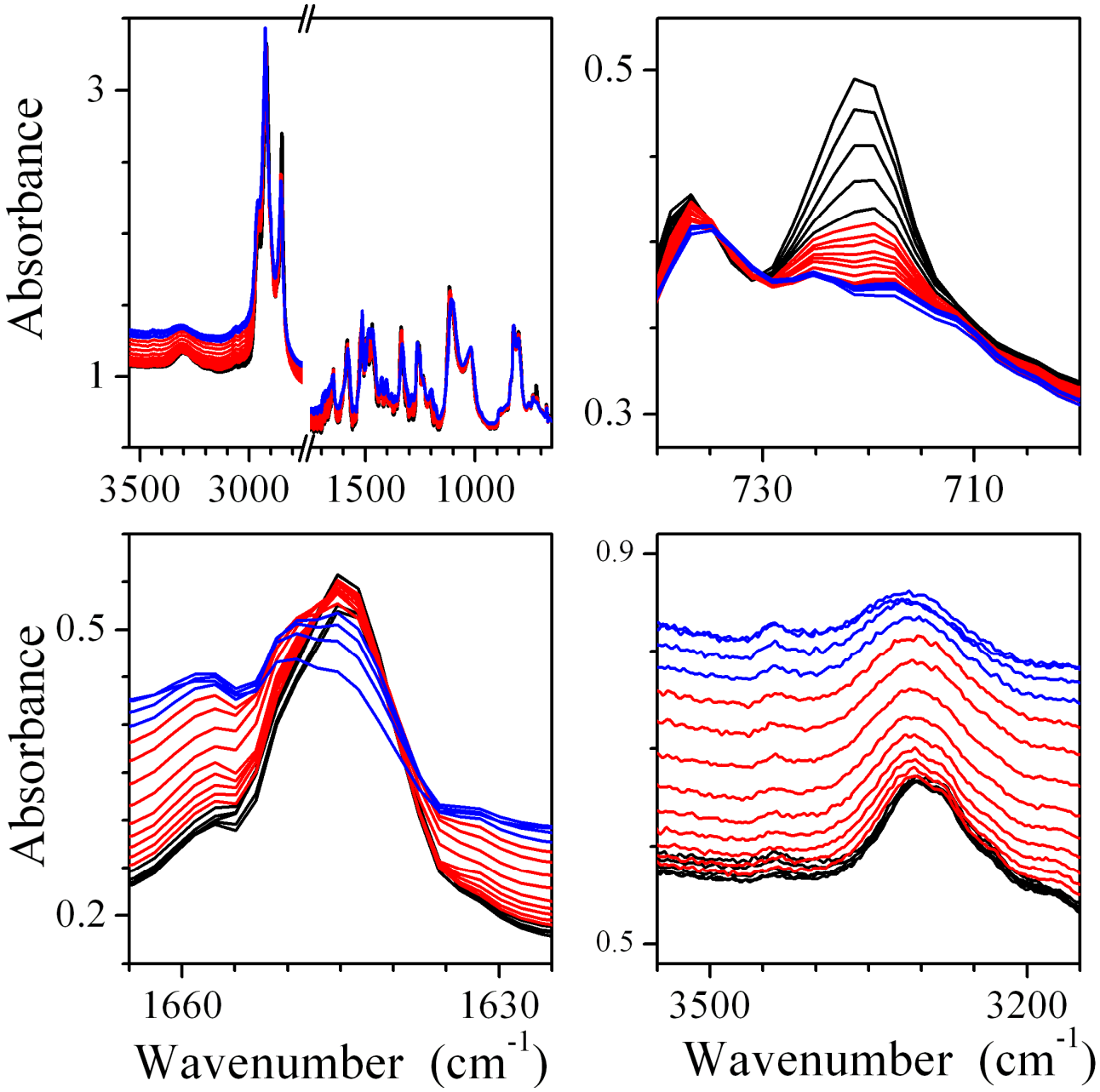

Figure 6. Solid-state IR absorption spectra of compound **1** (2% in KBr pellet) at the following temperatures (2nd heating): 20, 30, 40, 50 and 60°C (room temperature state, black lines), 70, 80, 90, 100, 110, 120, 130, 140 and 150°C (lamellar mesophase, red lines), 160, 170, 180 and 190°C (rectangular mesophase, blue lines). Graph up, left: superposition of spectra; up, right: amide V region with vibration modes of N-H···O bridges; down, left: amide I region with C=O stretching vibration; down, right: N-H stretching region.

The mechanism that leads to the interruption of half of the tert-butyl groups is a consequence

of the difference between the sections of InF bearing the TBF moieties, on the one hand, and the EPBA fragments, on the other hand. The folding of the mobile extremities of the EPBA fragments permits to fill the available volume whilst enhancing the segregation, and the maximum of efficiency occurs when the folding occurs towards a same layer containing the tert-butyl groups, starting in a random direction first, thus expelling the other half TB layers outside the columns to be mixed with the aliphatic continuum. Then, as in a germ growth crystallization process, the next layer is automatically selected as a row of column, and is continued until it reaches another growth domain.

Solid State luminescence properties

Luminescence properties of compound **1** in the various material states detected by DSC and SAXS were investigated with the help of a fluorescence microscope equipped with a heating stage and a UV-Vis-NIR spectrophotometer based on CCD detection technology. Fluorescence microscopy was found to be a powerful tool to probe the molecular organization in thin films at the macroscopic scale.[12, 20]

At temperatures above 225 °C, in the isotropic liquid, the luminescence appears light blue and completely uniform inside the fluid material in which all the molecules are randomly distributed. It is interesting to note that the luminescence remains very strong even at such high temperatures. The fluorescence spectra obtained above 225 °C displays a broad structureless emission band centred at 492 nm (Figure 8). In the bulk, the emission spectra are, as expected, broader and much less resolved than in solution (Figure 2) and the maxima are red-shifted by 82 nm. The difference should come from some remaining intermolecular interactions in the isotropic state, whilst the interactions with the solvent dominate in the solutions. Upon cooling, the birefringent domains of the rectangular mesophase readily develop, as observed by POM (Figure 3a). Interestingly, under irradiation at $340 < \lambda ex < 380$

nm (Hg lamp), the luminescence coming from the rectangular mesophase appears dark-blue and is clearly different from that one of the isotropic phase (Figure 7). Evidently, **1** is a thermochromic material, which exhibits temperature induced luminescence changes.[21] Spectroscopic measurements show that the colour change is due to an enhanced contribution of the two vibronic peaks at 443 and 468 nm (Figure 8). Temperature-dependent solid state absorption spectroscopy reveals that the absorption band remains unchanged between the isotropic phase and the rectangular phase (Figure S8). So, the luminescence modulation observed is not due to a slight bathochromic shift or enlargement of absorption band in the isotropic phase causing a re-absorption of the fluorescence at the higher energy side. This modulation can likely be explain by an exaltation of these two low-energy vibronic peaks from the emission profile is likely due to the organisation of the molecules into an anisotropic medium leading to specific orientation of between the transition dipole moments with the excitation beam.[22] Upon further cooling down to room temperature, the intensity of the luminescence at the higher energy side continuously increases down to room temperature, but without significant change of the uniform dark-blue fluorescence texture between both mesophases.

The unsubstituted compound DSF-IF(t-Bu)$_4$ shows an emission band displaying two maxima at 358 and 368 nm in solid state at room temperature (Figure S9), shifted by 10 nm compared to the solution spectrum, indicative of weak interactions in solid state. With compound **1** bearing the terminal N-(ethynylphenyl) benzamide (EPBA) fragments, the maxima in solid state (443, 468 and 492 nm) are shifted by more than 30 nm compare to those in solution (411, 435 and 467 nm). This large red-shift clearly indicates that the EPBA pendant units allow a more efficient π-π stacking in solid state.

To sum up, the luminescence properties of **1** are sensitive to the organisation inside the liquid crystalline state and the emission intensity and colour can be modulated with the temperature.

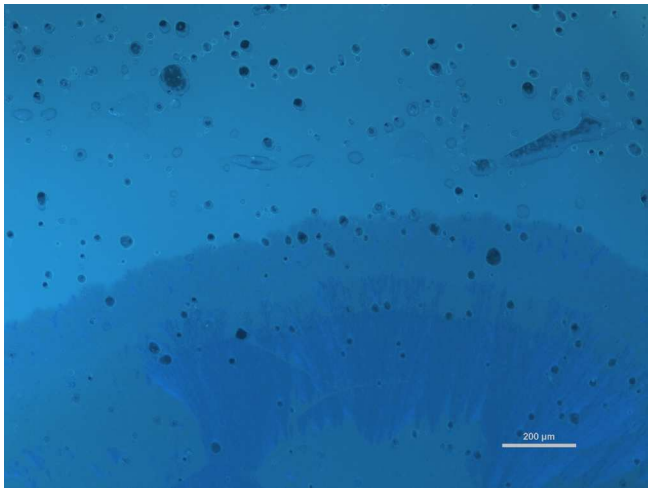

Figure 7. Co-existing isotropic liquid (light-blue) and HT (dark-blue) phases at 195 °C observed upon irradiation at $340 < \lambda_{ex} < 380$ nm (black areas correspond to trapped air bubbles) (same area as in Figure 3a).

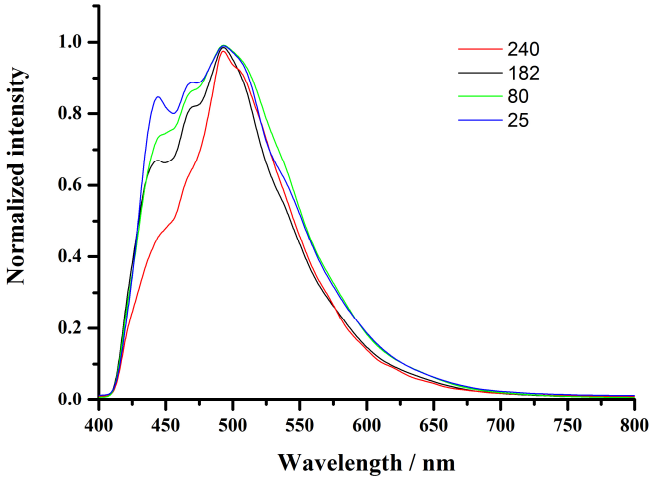

Figure 8. Bulk emission spectra of the compound **1** in a slender piece of glass at 240 °C in the isotropic liquid, at 182 °C in the rectangular mesophase, at 80 °C in the lamellar phase and at 25 °C in the poorly-organized room-temperature phase under excitation at 340-380 nm.

Modulation and polarization of the photoluminescence

The strong molecular anisotropy of the rod-shaped compound **1** (length = 7.7 nm; diameter = 1.3 nm) led us to explore the possibility to modulate and to polarize the photoluminescence

intensity using a nematic liquid crystalline host. For this purpose, compound **1** was dissolved in the nematic liquid crystal 5CB. It was found that **1** is well soluble in 5CB and the nematic phase of the LC host and the $T_{N/I}$ transition temperature (Figure S10) are weakly affected up to 1 weight%. Observations by polarizing microscopy and under UV irradiation confirmed the homogeneity of the LC mixtures and stability over several months. In contrast, the parent compound DSF-IF(t-Bu)$_4$, without the flexible pendant units, is not soluble in 5CB. Even the evaporation of dichloromethane solutions containing DSF-IF(t-Bu)$_4$/5CB mixtures also led to the formation of heterogenous suspensions. A crucial role of the flexible pendant units is to insure good solubility and stability in 5CB.

The LC mixture was introduced by capillarity in a LC cell with a 5 µm gap between the ITO coated glass (1 cm× 1cm). The polyimide (PI) layers on both ITO surfaces were rubbed in one-direction in an antiparallel alignment. The cell was then observed by optical microscopy without using a polarizer (Figure 9a). A voltage of 20 V was requested to switch the orientation of 5CB molecules in the direction perpendicular to the windows.

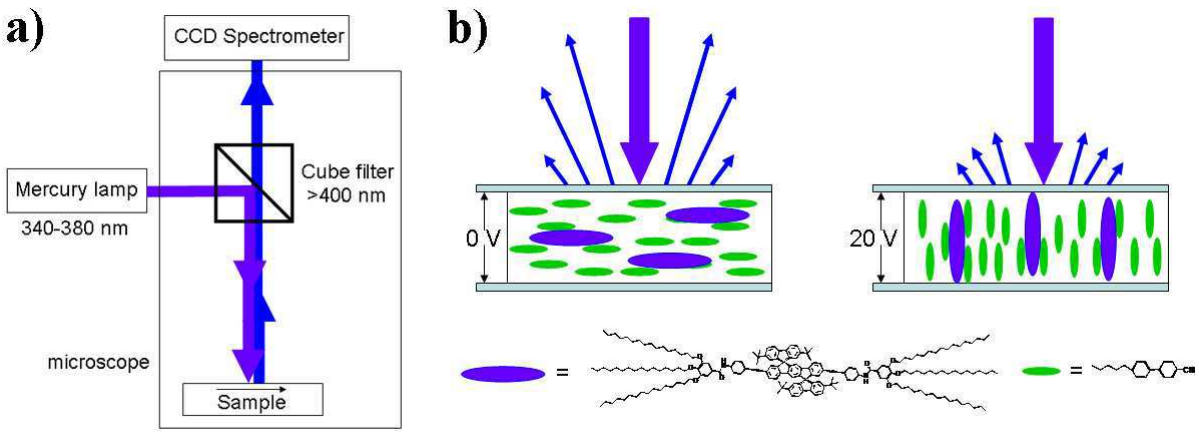

Figure 9. (a) Experimental setup for polarized photoluminescence measurements with compound **1**/5CB mixtures; (b) Schematic representation of the molecular organisation inside the LC cell without and with applied electric field and effect on the emitted blue light.

As the voltage is OFF, the molecules of **1** are parallel to the cell windows and a strong blue luminescence is observed (Figure 9b, left). The **1**/5CB mixture displays a strong structured emission band, spanning from 400 to 650 nm, centred at 442 nm (Figure 10a). The position of the emission band, which is slightly red-shifted by 32 nm compared to the emission band in diluted solutions (Figure 2), together with a well-resolved emission profile confirms the good dispersion of the luminescent DSF-IF derivative in the LC host. It should be noted that with the short acquisition times used (100-500 ms), the luminescence of 5CB was not detected at all. As the voltage switches 'ON', the reorientation of the 5CB molecules stimulates a macroscopic orientation of the molecules of **1** with their long axes perpendicular to the cell window, as shown in Figure 8b, right. As a result of this reorientation, the observed PL intensity of **1** is reduced by ~ 40 % (Figure 10a). This remarkable fluorescence modulation appears to be much more marked than that observed for example with europium(III) complexes[23] and of the same order of magnitude to the one observed with inorganic CdSe/ZnS nanorods.[10d] These results demonstrate that, at the molecular scale, the excitation is more efficient when the electromagnetic wave is perpendicular to the long axis of the dihydro(1,2-*b)*Indenofluorene core. The PL intensity instantaneously (< 1s) increases again when the voltage switches 'OFF'. The reversible switching of intensity in response to several cycles of field-off (0 V) and field-on (20 V) is presented in Figure 10b. The electric field was switched manually with an arbitrary period. It can be seen that the PL intensity quickly reaches to maximum during the field-on state while it goes to minimum in field-off state. This electrically switchable and repeatable photoluminescence modulation observed shows that the luminescent compound **1** can be efficiently used in optical switches.

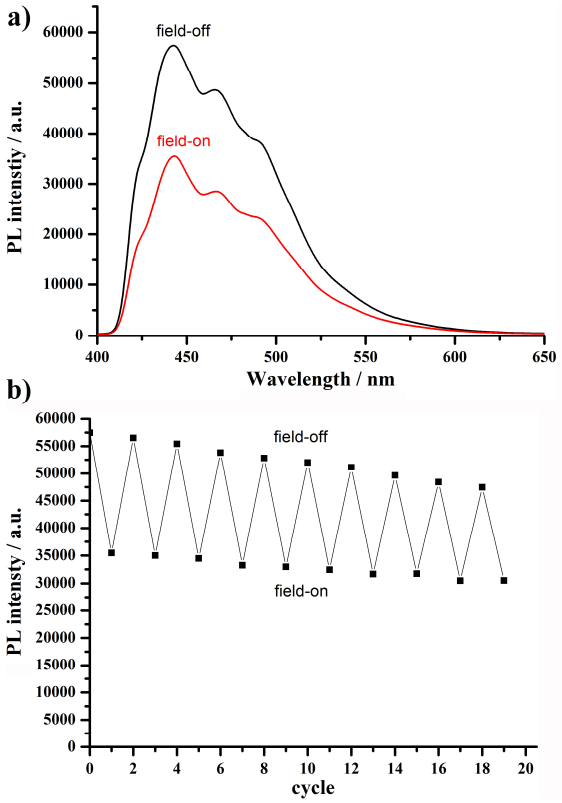

Figure 10. a) Emission spectra measured in field-off (0V) and field-on (20V); b) Time-dependent switching of PL intensity in response to several cycles of field-off (0V) and field-on (20V) (λ_{ex} =340-380 nm) ([**1**] = 0.1 %w/w in 5CB).

The ability of the aligned **1**/5CB mixture to generate polarized emission was also evaluated. For this purpose, an analyser was inserted between the CCD spectrometer and the cube filter. Without bias, the long molecular axis of molecule is oriented along rubbed PI direction with a planar anchoring parallel to the surface (Figure 9b, 0V). The photoluminescence intensity was evaluated as a function of the angle between the analyzer and the rubbed direction. At 0°, the analyzer's axis is parallel to the long molecular axis of **1** and perpendicular at 90°. As can be seen in Figure 11, the aligned **1**/5CB sample shows a strong angular dependence of photoluminescence intensity coming from **1**. These measurements clearly show that the intensity of the photoluminescence spectra is much larger in the parallel configuration than in the perpendicular one. The degree of polarization can be calculated by $\rho = (I// - I\perp)/(I// + I\perp)$,

where *I*// and *I*⊥ represent the polarization parallel (0°) and perpendicular (90°) to the rubbed PI direction, respectively. The resulting polarization ratio of 0.3 comparable with the values determined for polycatenar oligothiophenes.[24]

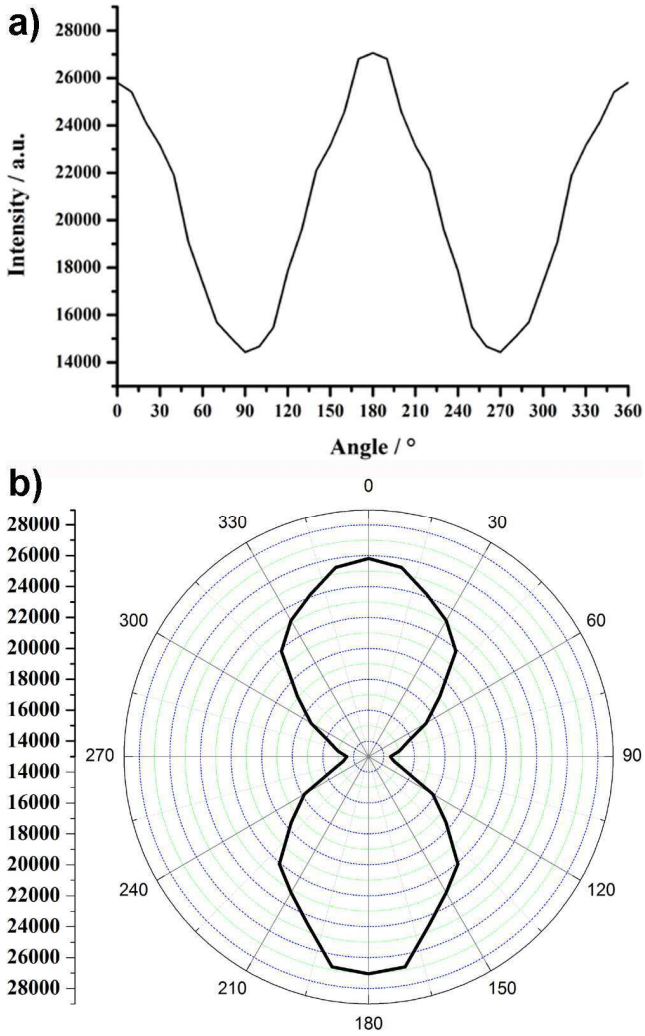

Figure 11. a) Photoluminescence intensity as a function of analyzer angle; b) Polar graph presentation. The excitation wavelength is 340-380 nm and the registration wavelength is 442 nm.

These results illustrate for the first time that aligned samples of DSF-IF derivatives can emit polarized light and that modulation of the luminescence can be induced by application of electric fields. The large structural anisotropy of **1** coupled to its good solubility in liquid

crystalline medium makes this class of compounds suitable for optical applications in LC devices.

Conclusion

The grafting of N-(ethynylphenyl) benzamide (EPBA) fragments carrying hexadecyl carbon chains on the bulky DSF-IF core has allowed the emergence of strongly luminescent liquid crystalline phases. Three different supramolecular organizations were revealed, starting namely with an initial poorly-organized phase, followed by a first transformation into a lamellar phase, and a second transition into a columnar mesophase. Based on variable-temperature SAXS measurements and on the crystalline structure of a parent molecule, models of the various molecular organizations were proposed. In the columnar phase, two supramolecular dimers, created through the piling of dihydro(1,2-*b)*Indenofluorene fragments, are organized in a disk-like repeat unit with half of the tert-butyl groups trapped in the centre and the rest of the tert-butyl fragments mixed with the long aliphatic chains arranged around the columns. The piling of these self-assembled units leads to the formation of “hollow” columns self-organizing in a rectangular lattice. The transition to the lamellar phase at low temperature is explained by the opening of the columns through the unfolding of the EPBA extremities. The thermal transitions are driven by steric constraints and by the dynamic of the hydrogen bonding networks. Temperature-dependent solid-state luminescence measurements have also revealed that this compound displays thermochromic luminescence properties with a marked photoluminescence colour change at the isotropic liquid-to-Col_{rec} phase transition. The functionalized DSF-IF core could also be dissolved in the nematic liquid crystal 5CB and switching of the photoluminescence emission could be realized in aligned samples or by applying electrical fields to a LC cell. Such highly functional materials are very appealing for

applications in optoelectronic requiring the generation or the control of light under electrical stimuli. DSF-IF derivatives with different molecular topologies are currently under investigations.

Acknowledgments

FC, CP, BD and BH thank the CNRS for its financial support. The ANR is also gratefully acknowledged for the PhD funding of ST. CP and ST thank the CINES for computing time. Nicolas Beyer is warmly acknowledged for his technical assistance in the temperature-dependent measurements.

Keywords. DSF-IF, luminescence modulation, Liquid crystal, LC device, Self-assembly

Experimental part.

General. 300 (^{1}H) and 75.5 MHz (^{13}C) NMR spectra were recorded on Bruker Avance 300 spectrometer at room temperature using perdeuterated solvents as internal standards. FT-IR spectra were recorded using a Varian-640 FT-IR spectrometer equipped with a PIKE ATR apparatus. High Resolution Mass Spectra were recorded with Varian MAT 311 instrument by the Centre Régional de Mesures Physiques de l'Ouest, Rennes. UV-visible spectra were recorded using an UV-Visible spectrophotometer SHIMADZU UV-1605. The UV-visible spectra were recorded using an UV-Visible spectrophotometer SHIMADZU UV-1605. Dichloromethane (analytical grade, VWR) was used without further purification. The optical gap was calculated from the absorption edge of the UV-vis absorption spectrum using the formula ΔE^{opt} (eV) = hc/λ, λ being the absorption edge (in meter). With h = 6.6x10^{-34} J.s (1eV = 1.6x10^{-19} J) and c = 3.0x10^{8} m.s^{-1}, this equation may be simplified as: ΔE^{opt} (eV) = 1237.5/λ (in nm). Photoluminescence spectra were recorded with a PTI spectrofluorimeter (PTI-814 PDS, MD 5020, LPS 220B) using a xenon lamp. Quantum yields in solution (ϕsol) were

calculated relative to quinine sulfate (ϕref = 0.546 in H_2SO_4 1N). ϕsol was determined according to the following equation,

$$\phi sol = \phi ref \times 100 \times [(Ts \times Ar)/(Tr \times As)] \times [(ns/nr)^2]$$

where, subscripts s and r refer respectively to the sample and reference. The integrated area of the emission peak in arbitrary units is given as T, n is the refracting index of the solvent (n_s = 1.421 for dichloromethane) and A is the absorbance. 3 solutions of different concentration of the substrate (A<0.1) were prepared and 3 solutions of the reference (quinine sulfate). The quinine sulfate concentration was chosen so as the absorption of the reference and the substrate were the same at the excitation wavelength. 3 quantum yields are then calculated at this wavelength and the average value is reported.

Variable-temperature FT-IR absorption spectra were performed on KBr pellets, by using a spectrometer Digilab FTS3000 and a home-built oven with an accuracy of 0.1°C. UV-visible spectra were recorded on µm-thick films between quartz glass slides, by using a spectrometer Agilent Cary 100 and a home-built oven with an accuracy of 0.1°C.

Optical microscopy investigations were performed on a Nikon H600L polarising microscope equipped with a Linkam "liquid crystal pro system" hotstage. The microscope is also equipped with a UV irradiation source (Hg Lamp, λ = 340-380 nm) and an ocean optic USB 2000+ UV-Vis-NIR spectrophotometer based on CCD detection technology. This set-up allows the recording of luminescence spectra on solids, liquids, liquid crystalline materials and gels from -196°C up to 420°C between 350 and 1100 nm. For electro-optical measurements, compound **1** was dissolved in the 4-cyano-4′-n-pentyl-1,1′-biphenyl (5CB) nematic liquid crystal and the LC mixture was introduced into a pre-assembled LC cell provided by Linkam (5 µm gap, capillary fill, ITO coated and anti parallel alignment). 5CB (>98 %) was purchased from TCI Europe and used without further purification. The voltage was applied with a standard potentiostat. Differential scanning calorimetry (DSC) was carried

out by using NETZSCH DSC 200 F3 instrument equipped with an intracooler. DSC traces were measured at 10 °C/min down to -30 °C. The XRD patterns were obtained with a transmission Debye-Scherrer-like geometry. A linear focalized monochromatic Cu-Kα_1 beam (λ = 1.5405Å) was obtained using a sealed-tube generator (600W) equipped with a bent quartz monochromator. In all cases, the crude powder was filled in Lindemann capillaries of 1mm diameter and 10 μm wall-thickness. The diffraction patterns were recorded with a curved Inel CPS120 counter gas-filled detector linked to a data acquisition computer (periodicities up to 70Å) and on image plates scanned by STORM 820 from Molecular Dynamics with 50μm resolution (periodicities up to 120Å). The sample temperature was controlled within ±0.01°C and exposure times were varied from 1 to 24h.

Full geometry optimization were performed with Density Functional Theory (DFT)[25,26] and Time-Dependent Density Functional Theory (TD-DFT) calculations were performed with the hybrid Becke-3 parameter exchange[27,28,29] functional and the Lee-Yang-Parr non-local correlation functional[30] (B3LYP) implemented in the Gaussian 09 (Revision B.01) program suite[31] using the 6-311G+(d,p) basis set and the default convergence criterion implemented in the program. The figures were generated with GaussView 5.0.

2',8'-dibromo-2,2",7,7"-tetrakis(1,1-dimethylethyl)-Dispiro[9*H*-fluorene-9,6'(12'*H*)-indeno[1,2-*b*]fluorene-12',9"-[9*H*]fluorene] (**DSF-IF(*t*-Bu)$_4$Br$_2$**) was synthesized as previously described.2 The synthesis and the characterization of the precursor **DSF-IF(*t*-Bu)$_4$** can be found in previous works.[14]

Compound 1: A schlenk flask was charged with DSF-IF(*t*-Bu)$_4$Br$_2$ (0.023 g, 0.024 mmol) and 2 equiv. N-(4-ethynylphenyl)-3,4,5-tris(hexadecyloxy)benzamide (0.057 g, 0.060 mmol)

and n-propylamine (10 mL). The mixture was degassed with argon. $Pd(PPh_3)_4$ (10 mg) was then added and the mixture was stirred at 60 °C overnight. The solvent was evaporated in vacuo, water was added to the residue and the product was extracted with dichloromethane. The organic layer was washed with water and filtered over hygroscopic cotton wool and evaporated. The residue was purified by column chromatography on silica gel using CH_2Cl_2 as eluent. The residue was precipitated from dichloromethane/methyl alcohol to give 0.030 g (46 %) of white solid. ^{1}H NMR ($CDCl_3$, 300 MHz, ppm) δ 7.80 (4H, d, *J* = 7.8, ArH), 7.68 (s, 2H, NH), 7.62-7.51 (m, 6H, ArH + ABsys), 7.50-7.36 (m, 10H, ArH + ABsys), 7.19 (s, 2H, ArH), 7.00 (s, 4H, ArH), 6.86 (s, 2H, ArH), 6.74 (4H, d, *J* = 1.8 Hz, ArH), 4.10-3.95 (m, 12H, OCH_2), 1.90-1.64 (m, 12H, CH_2), 1.57-1.39 (m, 12H, CH_2), 1.39-1.25 (m, 144H), 1.19 (s, 36H, CH_3 (tBu)), 0.90-0.85 (m, 18H, CH_3); ^{13}C NMR ($CDCl_3$, 75 MHz, ppm) δ 165.6 (C=O), 153.4 (Cq), 151.1 (Cq), 150.2 (Cq), 148.6 (Cq), 141.8 (Cq), 141.75 (Cq), 141.5 (Cq), 139.4 (Cq), 138.0 (Cq), 132.4 (CH), 131.2 (CH), 129.8 (Cq), 127.1 (CH), 125.25 (CH), 120.9 (CH), 120.3 (CH), 119.75 (CH), 119.4 (CH), 116.1 (CH), 105.9 (CH), 90.2 (C≡C), 73.7 (OCH_2), 69.6 (OCH_2), 66.1 (Cspiro), 35.0 (Cq), 32.1 (CH_2), 31.6 (CMe), 30.45 (CH_2), 29.9 (CH_2), 29.816 (CH_2), 29.7 (CH_2), 29.5 (CH_2), 26.2 (CH_2), 22.8 (CH_2), 14.3 (CH_3); HRMS (ESI^+, CH_2Cl_2/CH_3OH: 70/30) : Found : 2681.0530 (0 ppm) [M+Na]+, 1040.8409 (0 ppm) [M2+Na]+, 964.8106 (1 ppm) [M3+Na]+; required for $C_{186}H_{268}N_2O_8$: 2658.06; IR (ATR, cm^{-1}) ν = 3302 (NH), 2955, 2919, 2851, 1646 (C=O), 1581, 1515, 1494, 1467, 1426, 1404, 1362, 1336, 1291, 1260, 1237, 1206, 1180, 1115, 1020, 820. UV-vis (CH_2Cl_2): λ nm (ε, $M^{-1}.cm^{-1}$) 341 (79000), 379 (110000), 399 (113000).

[1] (a) J. Salbeck, N. Yu, J. Bauer, F. Weissörtel, H. Bestgen, *Synth. Met.* 1997, **91**, 209-215. (b) T. P. I. Saragi, T. Spehr, A. Siebert, T. Fuhrmann-Lieker, J. Salbeck, *Chem. Rev.* 2007, **107**, 1011-1065.

[2] D. Thirion, J. Rault-Berthelot, L. Vignau, C. Poriel, *Org. Lett.* 2011, **13**, 4418-4421.

[3] D. Horhant, J.-J. Liang, M. Virboul, C. Poriel, G. Alcaraz, J. Rault-Berthelot, *Org. Lett.* 2006, **8**, 257-260.

[4] C. Poriel, J.-J. Liang, J. Rault-Berthelot, F. Barrière, N. Cocherel, A. M. Z. Slawin, D. Horhant, M. Virboul, G. Alcaraz, N. Audebrand, L. Vignau, N. Huby, G. Wantz, L. Hirsch, *Chem. Eur. J.* 2007, **13**, 10055-10069.

[5] C. Poriel, J. Rault-Berthelot, D. Thirion, *J. Org. Chem.* 2013, **73**, 886-898.

[6] C. Poriel, N. Cocherel, J. Rault-Berthelot, L. Vignau, O. Jeannin, *Chem. Eur. J.* 2011, **17**, 12631-12645.

[7] M. Romain, D. Tondelier, J.-C. Vanel, B. Geffroy, O. Jeannin, J. Rault-Berthelot, R. Métivier, C. Poriel, *Angew. Chem. Int. Ed.* 2013, accepted 10.1002/anie.201306668.

[8] D. Thirion, M. Romain, J. Rault-Berthelot, C. Poriel, *J. Mater. Chem.* 2012, **22**, 7149-7157.

[9] (a) C. Weder, C. Sarwa, A. Montali, C. Bastiaansen, P. Smith, *Science* 1998, **279**, 835-837; (b) M. Irie, T. Fukaminato, T. Sasaki, N. Tamai, T. Kawai, *Nature* 2002, **420**, 759-760; (c) X. Zhang, S. Rehm, M. M. Safont-Sempere, F. Würthner, *Nat. Chem.* **2009**, *1*, 623-629; (d) T. Mutai, H. Satou, K. Araki, *Nat. Mater.* 2005, **4**, 685-687; (e) Y. Sagara, T. Kato, *Nat. Chem.* 2009, **1**, 605-610.

[10] (a) X. Tong, Y. Zhao, *J. Am. Chem. Soc.* 2007, **129**, 6372-6373; (b) R. Ozaki, T. Matsui, M. Ozaki, K. Yoshino, *Appl. Phys. Lett.* 2003, **82**, 3593-3595; (c) Y. M. Huang, W. Ge, J. W. Y. Lam, B. Z. Tang, *Appl. Phys. Lett.* 2001, **78**, 1652-1654; (d) M. V. Mukhina, V. V. Danilov, A. O. Orlova, M. V. Fedorov, M. V. Artemyev, A.V. Baranov, *Nanotechnology* 2012, **23**, 325101/1-325101/6.

[11] X. Tong, Y. Zhao, B. K. An, S. Y. Park, *Adv. Funct. Mater.* 2006, **16**, 1799-1804.

[12] S. Diring, F. Camerel, B. Donnio, T. Dintzer, S. Toffanin, R. Capelli, M. Muccini, R. Ziessel, *J. Am. Chem. Soc.*, 2009, **131**, 18177-18185.

[13] (a) D. Thirion, J. Rault-Berthelot, L. Vignau, C. Poriel, *Org. Lett.*, 2011, **13**, 4418-4421; (b) Y. Sagara, T. Kato, *Angew. Chem., Int. Ed.* **2011**, 50, 9128-9132.

[14] C. Poriel, J. Rault-Berthelot, F. Barrière, A. M. Z. Slawin, *Org. Lett.* 2008, **10**, 373-376.

[15] G. Heimel, M. Daghofer, J. Gierschner, E. J. W. List, A. C. Grimsdale, K. Müllen, D. Beljonne, J. L. Brédas, E. Zojer, *J. Chem. Phys.* 2005, **122**, 054501-054511.

[16] B. Valeur, *Molecular Fluorescence: Principles and Applications.*, Wiley-VCH Verlag GMbH & Co. KGaA, Weinheim, 2001.

[17] B. Donnio, B. Heinrich, H. Allouchi, J. Kain, S. Diele, D. Guillon, D. W. Bruce, *J. Am. Chem. Soc*. 2004, **126**, 15258–15268.

[18] D. J. Skrovanek, S. E. Howe, P. C. Painter, M. M. Coleman, *Macromolecules* 1985, **18**, 1676-1683.

[19] A. Barth, Ch. Zscherp, *Quarterly Reviews of Biophysics* 2002, **35**, 369–430.

[20] (a) F. Camerel, L. Bonardi, P. Retailleau, R. Ziessel, *J. Am. Chem.Soc.* 2006, **128**, 4548-4549; (b) F. Camerel, L. Bonardi, G. Ulrich, L. Charbonnière, B. Donnio, C. Bourgogne, D. Guillon, P. Retailleau, R. Ziessel, *Chem. Mater.* 2006, **18**, 5009-5021; (c) F. Camerel, G. Ulrich, J. Barbera, R. Ziessel, *Chem.-Eur. J.* 2007, **13**, 2189-2200; (d) K. Binnemans, *J. Mater. Chem.* 2009, **19**, 448-453.

[21] (a) S. Yamane, Y. Sagara, T. Kato, *Chem. Commun.* 2009, 3597-3599; (b) J. Liang, Z. Chen, J. Yin, G.-A. Yu, S. H. Liu, *Chem. Commun.* 2013, **49**, 3567-3569; (c) S.-J. Yoon, J. H. Kim, K. S. Kim, J. W. Chung, B. Heinrich, F. Mathevet, P. Kim, B. Donnio, A.-J. Attias, D. Kim, S. Y. Park, *Adv. Funct. Mater.* 2012, **22**, 61–69.

[22] I. Roppolo, E. Celasco, A. Fargues, A. Garcia, A. Revaux, G. Dantelle, F. Maroun, T. Gacoin, J.-P. Boilot, M. Sangermano, S. Perruchas, *J. Mater. Chem.* 2011, **21**, 19106-19113.

[23] K. Driesen, C. Vaes, T. Cardinaels, K. Goossens, C. Görller-Walrand, K. Binnemans, *J. Phys. Chem. B* 2009, **113**, 10575–10579.

[24] (a) N.S. Saricftci, U. Lemmer, D. Vacar, A. J. Heeger, R. A. J. Janssen, *Adv. Mater.* 1996, **8**, 651-654; (b) M. Honma, T. Horiuchi, T. Nose, *J. Appl. Phys.* 2009, **106**, 014507; (c) T. Yasuda, H. Ooi, J. Morita, Y. Akama, K. Minoura, M. Funahashi, T. Shimomura, T. Kato, *Adv. Funct. Mater.* 2009, **19**, 411–419.

[25] P. Hohenberg, W. Kohn, *Phys. Rev.* 1964, **136**, B864-B871.

[26] R. G. Parr, W. Yang, Oxford University Press, New York, Oxford, 1989.

[27] A. D. Becke, *Phys. Rev. A.* 1988, **38**, 3098-3100.

[28] A. D. Becke, *J. Chem. Phys.* 1993, **98**, 5648-5652.

[29] A. D. Becke, *J. Chem. Phys.* 1993, **98**, 1372-1377.

[30] C. Lee, W. Yang, R. G. Parr, *Phys. Rev. B.* 1988, **37**, 785-789.

[31] M. J. Frisch, G. W. Trucks, H. B. Schlegel, G. E. Scuseria, M. A. Robb, J. R. Cheeseman, G. Scalmani, V. Barone, B. Mennucci, G. A. Petersson, H. Nakatsuji, M. Caricato, X. Li, H. P. Hratchian, A. F. Izmaylov, J. Bloino, G. Zheng, J. L. Sonnenberg, M. Hada, M. Ehara, K. Toyota, R. Fukuda, J. Hasegawa, M. Ishida, T. Nakajima, Y. Honda, O. Kitao, H. Nakai, T. Vreven, J. A. Montgomery, Jr., J. E. Peralta, F. Ogliaro, M. Bearpark, J. J. Heyd, E. Brothers, K. N. Kudin, V. N. Staroverov, R. Kobayashi, J. Normand, K. Raghavachari, A. Rendell, J. C. Burant, S. S. Iyengar, J. Tomasi, M. Cossi, N. Rega, J. M. Millam, M. Klene, J. E. Knox, J. B. Cross, V. Bakken, C. Adamo, J. Jaramillo, R. Gomperts, R. E. Stratmann, O. Yazyev, A. J. Austin, R. Cammi, C. Pomelli, J. W. Ochterski, R. L. Martin, K. Morokuma, V. G. Zakrzewski, G. A. Voth, P. Salvador, J. J. Dannenberg, S. Dapprich, A. D. Daniels, Ö. Farkas,

J. B. Foresman, J. V. Ortiz, J. Cioslowski, and D. J. Fox, Gaussian, Inc., Wallingford CT, 2009.